Measurements of the magnetic form factor of the proton for timelike momentum transfers

M. Andreotti,[b] S. Bagnasco,[c] W. Baldini,[b] D. Bettoni,[b] G. Borreani,[g] A. Buzzo,[c] R. Calabrese,[b] R. Cester,[g] G. Cibinetto,[b] P. Dalpiaz,[b] G. Garzoglio,[a] K. Gollwitzer,[a] M. Graham,[e] M. Hu,[a] D. Joffe,[f] J. Kasper,[f] G. Lasio,[d] M. Lo Vetere,[c] E. Luppi,[b] M. Macrì,[c] M. Mandelkern,[d] F. Marchetto,[g] M. Marinelli,[c] E. Menichetti,[g] Z. Metreveli,[f] R. Mussa,[b,g] M. Negrini,[b] M. Obertino,[g] M. Pallavicini,[c] N. Pastrone,[g] C. Patrignani,[c] S. Pordes,[a] E. Robutti,[c] W. Roethel,[f,d] J. Rosen,[f] P. Rumerio,[f] R. Rusack,[e] A. Santroni,[c] J. Schultz,[d] S. H. Seo,[e] K. K. Seth,[f] G. Stancari,[a,b] M. Stancari,[d,b] A. Tomaradze,[f] I. Uman,[f] T. Vidnovic III,[e] S. Werkema[a] and P. Zweber[f]

[a] *Fermi National Accelerator Laboratory, Batavia, Illinois 60510*

[b] *Istituto Nazionale di Fisica Nucleare and University of Ferrara, 44100 Ferrara, Italy*

[c] *Istituto Nazionale di Fisica Nucleare and University of Genova, 16146 Genova, Italy*

[d] *University of California at Irvine, California, 92697*

[e] *University of Minnesota, Minneapolis, Minnesota 55455*

[f] *Northwestern University, Evanston, Illinois 60208*

[g] *Istituto Nazionale di Fisica Nucleare and University of Torino, 10125 Torino, Italy*

Abstract

Fermilab experiment E835 has measured the cross section for the reaction $\overline{p}p \to e^+e^-$ at $s = 11.63$, 12.43, 14.40 and 18.22 GeV^2. From the analysis of the 66 observed events new high-precision measurements of the proton magnetic form factor are obtained.

Key words: nucleon, form factors
PACS: 13.40.Gp, 13.75.Cs, 14.20.Dh

The electromagnetic properties of the proton are studied by measuring the electric and magnetic form factors $G_E(q^2)$ and $G_M(q^2)$ as a function of the four-momentum transfer q^2. In the spacelike region ($q^2 < 0$) the electric and magnetic form factors of the proton have been measured in elastic electron-proton scattering up to $|q^2| = 10$ (GeV/c)^2 and $|q^2| = 31$ (GeV/c)^2, respectively. Experimental results for G_M in the timelike region ($q^2 > 0$) exist for $4m_p^2 \leq s \leq 14.4$ GeV^2.

In this paper we present results from new measurements of the cross section for the reaction $\overline{p}p \to e^+e^-$ in the interval 11.63 GeV$^2 \leq s \leq$ 18.22 GeV^2. The differential cross section for this process can be expressed in terms of the proton form factors as follows [1]:

$$\left(\frac{d\sigma}{d\Omega}\right)_{\overline{p}p\to e^+e^-} = \frac{\alpha^2}{4\beta_p s} \cdot \left[|G_M|^2 (1+\cos^2\theta^*) + \frac{4m_p^2}{s} |G_E|^2 \sin^2\theta^* \right], \quad (1)$$

where θ^* is the scattering angle of the electron in the center of mass (c.m.) system and β_p is the velocity of the proton (or antiproton) in the c.m.: $\beta_p = \sqrt{1-4m_p^2/s}$.

Fermilab experiment E835 is dedicated to the study of charmonium by resonant formation in $\overline{p}p$ annihilations. It is a fixed target experiment, in which the $\overline{p}$ beam circulating in the Accumulator intersects a hydrogen gas jet target. The form factor results for the data taken in the October 1996 through September 1997 run of E835 were reported in our earlier publication [2]. In this letter we report on the results obtained from the data taken during the January 2000 through November 2000 run of E835.

The E835 apparatus [3] is optimized for the detection of electromagnetic final states. It is a non-magnetic spectrometer with full azimuthal (ϕ) coverage and polar angle (θ) acceptance ranging from 2° to 70° in the lab frame. The central detector ($11° < \theta < 70°$) has cylindrical symmetry around the beam axis. Its main components are: the central tracking system (consisting of 3 scintillator hodoscopes, 2 straw chambers and 2 scintillating fiber trackers), a threshold Čerenkov counter for e/π discrimination and a central electromagnetic calorimeter (CCAL) made of 1280 leadglass blocks pointing to the interaction region. All CCAL channels are equipped with both time and pulse-height readout. The time measurements allow the rejection of signals from out-of-time events (accidental pileup).

The first level trigger for the e^+e^- final state requires two "electron" signals, each defined as the coincidence of the appropriate elements of the scintillator hodoscopes and the corresponding cells of the Čerenkov . Independently, the first level trigger requires two high-energy showers in CCAL with an azimuthal

opening angle greater than 90^o.

Events which satisfy the first level trigger are processed by the on-line filter, which selects events in which the two highest-energy clusters in CCAL have an invariant mass greater than 2.2 GeV/c^2.

Events are reconstructed off-line using all information from the central tracking detectors, the Čerenkov counter and the central calorimeter. The two electron candidates are identified as the tracks with the highest invariant mass. The selection of $\overline{p}p \to e^+e^-$ proceeds in four steps.

(a) *Electron identification.* For each candidate electron track a variable is constructed, called *Electron Weight* (EW), using the pulse heights in the scintillator hodoscopes and Čerenkov counter, second moments of the transverse shower distribution in CCAL and the fractional shower energy in 3×3 block region of CCAL [2]. EW is a likelihood ratio for the electron hypothesis versus background hypothesis. Since we search events with two electrons we use the product of the two *Electron Weights*. The distribution of $\log_{10}(ew1 * ew2)$ in a clean sample is shown in Fig. 1. In order to reduce the data sample size a pre-selection is applied requiring $\log_{10}(ew1 * ew2) > -1$ and an invariant mass of the two candidate electrons greater than 2.2 GeV/c^2. Only events which pass this pre-selection undergo the subsequent analysis. In the final selection we require $\log_{10}(ew1 * ew2) > 0$.

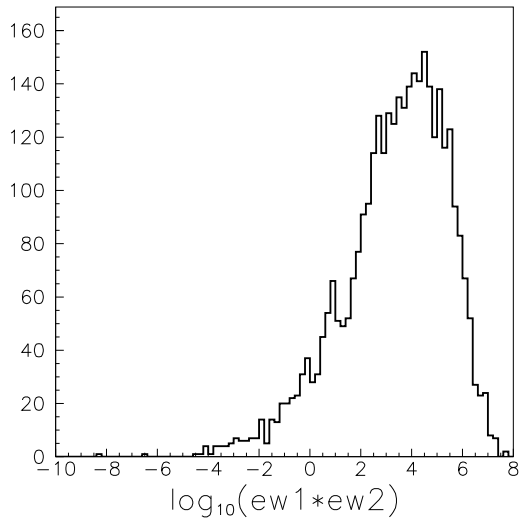

Fig. 1. Distribution of $\log_{10}(ew1 * ew2)$ for a sample of $\psi' \to e^+e^-$ events.

(b) *Fiducial volume.* To ensure homogeneity in the response of the detector we accept only events in which the two electrons have polar angles in the interval $15^o < \theta < 60^o$. This region is well covered by Central Calorimeter, Čerenkov counter and central tracking detectors.

(c) *CCAL multiplicity.* To avoid rejecting events in which the electron or positron radiates a Bremsstrahlung photon which forms a distinct cluster in the CCAL, we do not impose a strict cut demanding only two on-time clusters. Events with more than two on-time clusters are kept provided that the extra clusters, when paired with either electron candidate, give an invariant mass less than 100 MeV/c^2. In addition any number of out-of-time or undetermined clusters is allowed.

(d) *Kinematical fit.* The goodness of the e^+e^- final state is finally tested by means of a four-constraint kinematical fit. Since the energy range considered is near to charmonium resonances which decay into $J/\psi X$ we use also a kinematical fit to test the $J/\psi X$ final state, then we compare the fit probability for e^+e^- ($Prb(e^+e^-)$) with that for $J/\psi X$ ($Prb(J/\psi X)$). The event is accepted if $Prb(e^+e^-) > Prb(J/\psi X)$ and $Prb(e^+e^-) > 1\%$.

The number N of events selected with these criteria is shown in Table 1.

s (GeV^2)	L (pb^{-1})	N	σ_{acc} (pb)	$\lvert\cos\theta^*\rvert_{max}$	$10^2 \times \lvert G_M \rvert$ (a)	(b)
11.63±0.17	32.86	32	$1.61^{+0.34+0.17}_{-0.29-0.10}$	0.575	$1.74^{+0.18+0.11}_{-0.16-0.07}$	$1.94^{+0.20+0.12}_{-0.17-0.08}$
12.43±0.01	50.50	34	$1.11^{+0.23+0.12}_{-0.19-0.07}$	0.601	$1.48^{+0.15+0.08}_{-0.13-0.05}$	$1.63^{+0.17+0.09}_{-0.14-0.05}$
14.40±0.19	5.17	0	< 0.80	0.603	< 1.38	< 1.51
18.22±0.01	2.10	0	< 1.98	0.512	< 2.77	< 2.99

Table 1
Summary of the results of the form factor analysis. For each energy region the integrated luminosity L, the selected number of events N, the cross section $\sigma_{acc} = N/(\epsilon \cdot L)$ are reported. $\lvert\cos\theta^*\rvert_{max}$ is the maximum value of $\lvert\cos\theta^*\rvert$ where θ^* is the scattering angle in c.m.; (a) $|G_M|$ calculated in the hypothesis $|G_E| = |G_M|$; (b) $|G_M|$ calculated in the approximation of negligible electric contribution.

The overall efficiency of the analysis is the product of the three efficiencies corresponding to the first level trigger, the off-line preselection and the final selection. The efficiency of the restriction on the fiducial volume is taken into account in the integration of the differential cross section (1).

The trigger efficiency ϵ_{trig} has been calculated from special trigger runs at the ψ' energy, which required only one electron. The trigger efficiency is determined to be:

$$\epsilon_{trig} = 0.90 \pm 0.02 \tag{2}$$

The efficiency of the preliminary selection has been calculated using clean $\psi' \to e^+e^-$ events selected requiring only two on-time CCAL clusters and applying tight topological cuts relative to the two body final state. The value of the efficiency obtained with this method is:

$$\epsilon_{pres} = 0.950 \pm 0.012(stat)^{+0.013}_{-0.010}(syst) \tag{3}$$

The efficiency of the final selection was also calculated by means of clean $\psi' \to e^+e^-$ events. Fig. 2 shows e^+e^- invariant mass distributions for candidate events after preliminary selection (a) and after final selection (b) at the ψ' formation energy and off-resonance at $\sqrt{s} = 3.7$ GeV. The cross-hatched areas in both histograms correspond to the background contamination in these samples, extracted applying the same analysis to the data taken off resonance at $\sqrt{s} = 3.7$ GeV. Horizontal lines correspond to the decay $\psi' \to J/\psi X$ selected requiring $Prb(J/\psi X) > 1\%$ and $Prb(e^+e^-) < 10\%$. It can be seen that the background contamination from J/ψ-inclusive decay is very small.

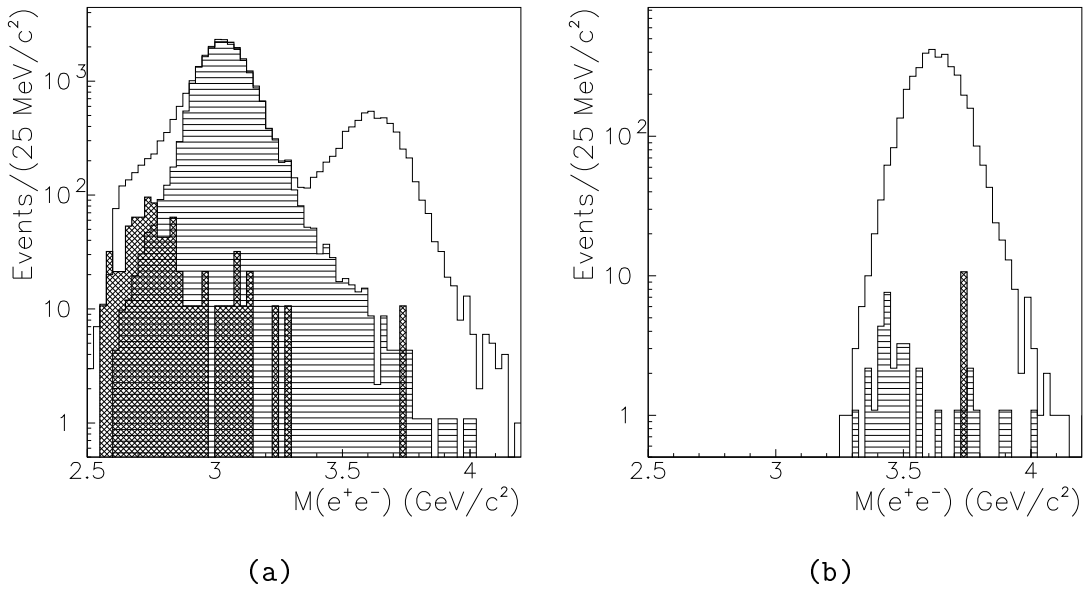

Fig. 2. Invariant mass distribution for e^+e^- candidate events, (a) after preliminary selection and (b) after final selection. Events at ψ' energy are shown as white histograms and those at $\sqrt{s} = 3.7$ GeV are shown as cross-hatched histograms. Horizontal lines correspond to J/ψ-inclusive subsample at ψ' energy. The number of events at $\sqrt{s} = 3.7$ GeV has been rescaled by integrated luminosity.

The efficiency of the final selection is defined as the fraction of events in the

preliminary sample (Fig. 2(a) white) that survive all cuts (Fig. 2(b) white), once background (including $J/\psi X$ events) is subtracted. We consider only events with invariant mass greater than 3.4 GeV/c^2. The efficiency of the final selection is:

$$\epsilon_{sel} = 0.706 \pm 0.009(stat)^{+0.046}_{-0.020}(syst) \tag{4}$$

The overall analysis efficiency is thus:

$$\epsilon_{ana} = 0.604 \pm 0.017(stat)^{+0.048}_{-0.023}(syst) \tag{5}$$

where the systematic error takes into account the variation of efficiency with time and the effect of the background subtraction procedure. The main possible sources of background for the e^+e^- final state are: photon conversions and π^0 Dalitz decays, two body hadronic final states (mainly $\pi^+\pi^-$) and $J/\psi X$ events. These background processes have been studied in detail and their contributions have been estimated to be as follows [2]:

(1) Photon conversions from $\overline{p}p$ decays to $\gamma\gamma$, $\pi^o\gamma$ and $\pi^0\pi^0$ and Dalitz decays. We estimate these processes to contribute backgrounds of $< 3.1 \times 10^{-3}$ pb and $< 1.7 \times 10^{-3}$ pb at $s = 11.63$ GeV^2 and 12.43 GeV^2 respectively.
(2) Misidentification of the $\pi^+\pi^-$ final state as e^+e^- . We estimate this process to contribute $< 4.3 \times 10^{-3}$ pb and $< 2.9 \times 10^{-3}$ pb at $s = 11.63$ GeV^2 and 12.43 GeV^2 respectively.
(3) Inclusive final state $J/\psi X \to e^+e^-$, with X not detected. The contribution of this process is estimated to be 1.6×10^{-2} pb and 1.0×10^{-2} pb at $s = 11.63$ GeV^2 and 12.43 GeV^2 respectively.

Comparing the estimated upper limits with the values of cross section reported in Tab. 1 we see that all background sources give a negligible contamination, therefore no subtraction from the number of candidate events is performed.

From the number N of selected events with an integrated luminosity L and an efficiency ϵ_{ana} the differential cross section integrated in the c.m. acceptance region can be calculated as follows:

$$\sigma_{acc} = \frac{N}{\epsilon_{ana} L} \tag{6}$$

σ_{acc} is a function of the magnetic and electric form factors G_M and G_E:

$$\begin{aligned} \sigma_{acc} &= \int_0^{2\pi} d\phi \int_{-|\cos\theta^*|_{max}}^{+|\cos\theta^*|_{max}} \frac{d\sigma}{d\Omega} d(\cos\theta^*) \\ &= \frac{\pi\alpha^2}{2\beta_p s} \cdot \left[A \cdot |G_M|^2 + \frac{4m_p^2}{s} \cdot B \cdot |G_E|^2 \right] \end{aligned} \tag{7}$$

where A and B are:

$$A = 2 \cdot \int_0^{+|\cos\theta^*|_{max}} (1 + \cos^2\theta^*) d(\cos\theta^*) \tag{8}$$

$$B = 2 \cdot \int_0^{+|\cos\theta^*|_{max}} (1 - \cos^2\theta^*) d(\cos\theta^*) \tag{9}$$

Since the small number of events and the limited $\cos\theta^*$ range do not allow us to measure the angular distribution, two alternative hypotheses have been made: (a) $|G_E| = |G_M|$, as at the threshold of the timelike region ($s = 4m_p^2c^4$); (b) the "electric" contribution is assumed to be negligible. Under these two hypotheses the expressions of $|G_M|$ are respectively:

$$(a) \quad |G_M| = \left[\frac{2\ \beta_p\ s\ \sigma_{acc}}{\pi\ \alpha^2\ \left[A + \frac{4m_p^2}{s} B\right]} \right]^{\frac{1}{2}} \tag{10}$$

$$(b) \quad |G_M| = \left[\frac{2\ \beta_p\ s\ \sigma_{acc}}{\pi\ \alpha^2\ A} \right]^{\frac{1}{2}} \tag{11}$$

Tab. 1 shows the results for the magnetic form factor of the proton calculated under the two hypotheses. An upper limit at the 90 % confidence level is reported where there are no observed events. The errors shown are respectively statistical and systematic. The systematic uncertainty is due to the errors on efficiency and luminosity. The values of $|G_M|$ obtained under hypothesis (a) are plotted in Fig. 3, where they are compared with earlier measurements. It can be seen that the new data are in excellent agreement with the previous E760 and E835 results.

Quantum Chromodynamics predicts an asymptotic behavior for the magnetic form factor of the proton in the timelike region at high energy of the form:

$$G_M(Q^2) = \frac{C}{s^2} \cdot \left(\ln \frac{s}{\Lambda^2} \right)^{-2} \tag{12}$$

where $\Lambda = 0.3$ GeV is the QCD scale parameter and C is a free parameter. This functional form comes from the prediction that for large momentum transfers $q^4|G_M|$ should be nearly proportional to the square of the running coupling constant for strong interactions $\alpha_s^2(q^2)$ [4,5]. The dashed line in Fig. 3 shows a fit to the data according to equation (12). As can be seen, the fit agrees well with the data over the q^2 range explored so far.

In summary, we have presented new, high-precision measurements of the proton magnetic form factor in the timelike region at large q^2. The results are in excellent agreement with previous measurements and with the semi-quantitative predictions of QCD.

The authors wish to acknowledge the technical support from their respec-

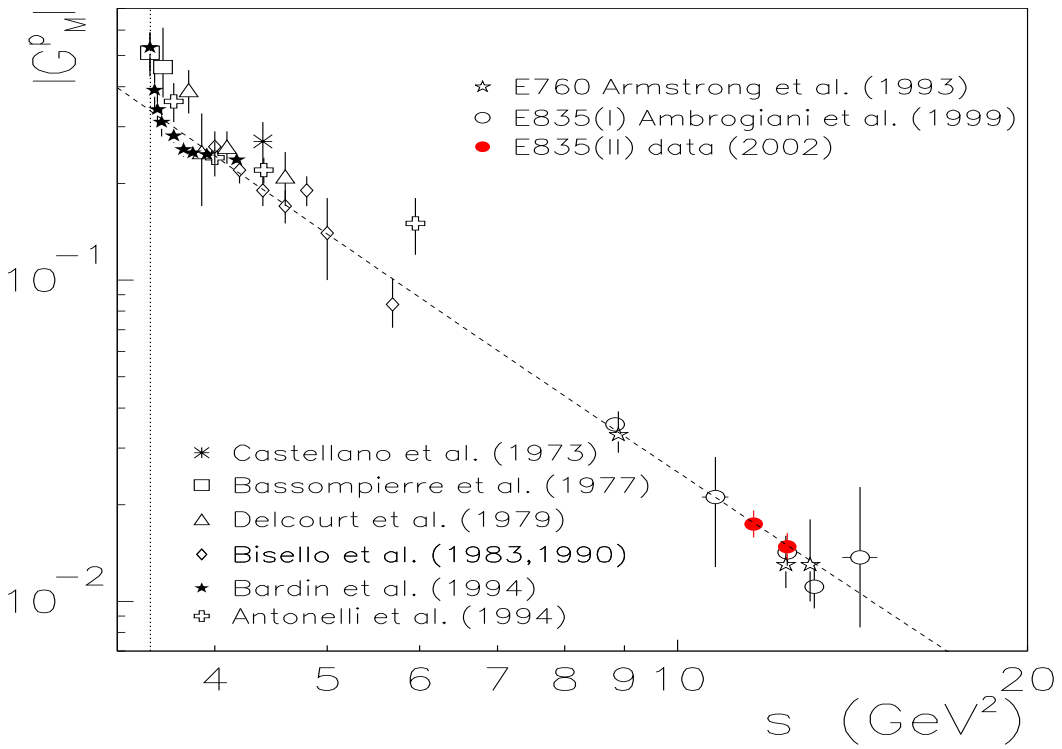

Fig. 3. All existing values of the magnetic form factor in timelike region obtained with the hypothesis $|G_M| = |G_E|$. For the earlier experiments see Ref. [2] and references therein.

tive institutions and the contribution of the Fermilab Beams Division. This research was supported by the U.S. Department of Energy and the Italian Istituto Nazionale di Fisica Nucleare.

References

[1] A. Zichichi et al., Nuovo Cimento **XXIV**, 170 (1962).

[2] M. Ambrogiani et al., Phys. Rev. D **60**, 032002 (1999).

[3] S. Bagnasco et al., Phys. Lett. B **533**, 237 (2002).

[4] G. Lepage and S. Brodsky, Phys. Rev. Lett. **43**, 545 (1979).

[5] G. Lepage and S. Brodsky, Phys. Rev. D**22**, 2157 (1980).